

# Modeling the impacts of point-source inputs on nitrogen retention in an urban river under low-flow conditions

Jingshui Huang<sup>1</sup>, Hailong Yin<sup>2</sup>, Seifeddine Jomaa<sup>1</sup>, Michael Rode<sup>1</sup>, and Qi Zhou<sup>2</sup>

<sup>1</sup>Department of Aquatic Ecosystem Analysis and Management, Helmholtz Centre for Environmental Research – UFZ, Brückstraße 3a, 39114 Magdeburg, Germany

<sup>2</sup>College of Environmental Science and Engineering, Tongji University, Shanghai 200092, China

November 24, 2022

## Abstract

Excessive dissolved inorganic nitrogen (DIN) added to the urban river systems by point-source inputs, such as untreated wastewater and wastewater treatment plant (WWTP) effluent, constitutes a water-quality problem of growing concern in China. However, very little is known about their impacts on DIN retention capacity and pathways in receiving waters. In this study, a spatially-intensive water quality monitoring campaign was conducted to support the application of the river water quality model WASP7.5 to the PS-impacted Nanfei River, China. The DIN retention capacities and pathway of a reference upstream Reach A, a wastewater-impacted Reach B and an effluent-dominated Reach C were quantified using the model results after a Bayesian approach for parameter estimation and uncertainty analysis. The results showed that the untreated wastewater discharge elevated the assimilatory uptake rate but lowered its efficiency in Reach B; while the WWTP effluent discharge elevated both denitrification rate and efficiency and made Reach C a denitrification hotspot with increased nitrate concentration and hypoxic environment. The effects of the point-source inputs on the DIN retention pathways (assimilatory uptake vs. denitrification) were regulated by their impacts on river metabolism. Despite different pathways, the total DIN retention ratios of Reaches A, B and C under low-flow conditions were 30.3% km<sup>-1</sup>, 14.3% km<sup>-1</sup> and 6.5% km<sup>-1</sup>, respectively, which indicated the instream DIN retention capacities were significantly impaired by the point-source inputs. This result suggests that the DIN discharged from point-source inputs to urban rivers will be transported downstream with the potential to create long-term ecological implications not only locally but also regionally.

# Modeling the impacts of point-source inputs on nitrogen retention in an urban river under low-flow conditions

Jingshui Huang <sup>1,2</sup>, Hailong Yin <sup>1,\*</sup>, Seifeddine Jomaa <sup>2</sup>, Michael Rode <sup>2</sup>, Qi Zhou <sup>1</sup>

<sup>1</sup> College of Environmental Science and Engineering, Tongji University, Shanghai 200092, China.

<sup>2</sup> Department of Aquatic Ecosystem Analysis and Management, Helmholtz Centre for Environmental Research – UFZ, Brückstraße 3a, 39114 Magdeburg, Germany.

\* Author to whom all correspondence should be addressed: [yinhailong@tongji.edu.cn](mailto:yinhailong@tongji.edu.cn);

## Abstract

Excessive dissolved inorganic nitrogen (DIN) added to the urban river systems by point-source inputs, such as untreated wastewater and wastewater treatment plant (WWTP) effluent, constitutes a water-quality problem of growing concern in China. However, very little is known about their impacts on DIN retention capacity and pathways in receiving waters. In this study, a spatially-intensive water quality monitoring campaign was conducted to support the application of the river water quality model WASP7.5 to the PS-impacted Nanfei River, China. The DIN retention capacities and pathway of a reference upstream Reach A, a wastewater-impacted Reach B and an effluent-dominated Reach C were quantified using the model results after a Bayesian approach for parameter estimation and uncertainty analysis. The results showed that the untreated wastewater discharge elevated the assimilatory uptake rate but lowered its efficiency in Reach B; while the WWTP effluent discharge elevated both denitrification rate and efficiency and made Reach C a denitrification hotspot with increased nitrate concentration and

hypoxic environment. The effects of the point-source inputs on the DIN retention pathways (assimilatory uptake vs. denitrification) were regulated by their impacts on river metabolism. Despite different pathways, the total DIN retention ratios of Reaches A, B and C under low-flow conditions were 30.3% km<sup>-1</sup>, 14.3% km<sup>-1</sup> and 6.5% km<sup>-1</sup>, respectively, which indicated the instream DIN retention capacities were significantly impaired by the point-source inputs. This result suggests that the DIN discharged from point-source inputs to urban rivers will be transported downstream with the potential to create long-term ecological implications not only locally but also regionally.

**Keywords** Nitrogen retention; denitrification; assimilatory uptake; wastewater; effluent; water quality modeling;

## 1. Introduction

Point source (PS) pollution, such as untreated wastewater and wastewater treatment plant (WWTP) effluent, contributes >50% of nitrogen (N) loads to receiving waters in urban areas (Carey and Migliaccio, 2009; Martí et al., 2010). In the past two decades, large-scale centralized WWTPs have been rapidly built in China (Yu et al., 2019). Almost all urban water bodies in China are faced with the challenge of receiving WWTP effluents, and some even become effluent-dominated (Huang et al., 2017). Although there has been an increasing trend to include tertiary treatment (i.e., chemical and biological removal of nutrients) in WWTPs in China, their effluent discharges may still cause abrupt changes of ambient N levels, and thus alter instream N processes in receiving waters (Martí et al., 2010). Besides, due to the uncompleted urbanization

process some untreated wastewaters are also sometimes distributed along urban rivers discharging N loadings in other forms than that in WWTP effluent. Despite the fact that PS inputs into urban rivers are widely spread, their impacts on instream N retention capacity and pathway have been hardly examined in China. Thus, clear need exists to understand how high nutrient loads from PSs affect the instream N retention capacity and pathways of urban rivers in China, where anthropogenic N discharge to freshwater far exceeds its 'safe' threshold (Yu et al., 2019). Pristine streams are widely believed to have a high N retention capacity (Peterson et al., 2001). This intrinsic 'self-purifying' characteristic could help alleviate water-quality problems by regulating N downstream export. However, the N retention capacity of streams receiving higher N loading from PS is suggested to be impaired in some studies (Gibson and Meyer, 2007; Haggard et al., 2005). These studies claimed that the streams below PSs export N without significant net retention or lower processing efficiency. In contrast, results from other studies have shown either no significant effect or even an increase in N retention capacity at sites downstream from PSs (Gücker et al., 2006; Rahm et al., 2016). In these cases, point sources may act as 'point sinks' by enhancing instream N processing in receiving waters. The variability of conclusions reflects the influence of different controlling factors among site-specific studies. The controlling factors include both effluent- and ambient-related ones, e.g. the nitrate/ammonium ratio of the effluent, which depends on the wastewater treatment type and effectiveness, the ratio of effluent discharge to river flow, availability of phosphorus, concentrations of oxygen and dissolved organic carbon, etc. The complexity of controlling factors emphasizes the importance of assessing the N retention capacity in urban rivers receiving PS inputs in China, where the characteristics of effluent and receiving waters are different from those most published in developed countries.

Besides, the results are expected to provide evidences for an ongoing debate on whether to invest in WWTP upgrade to further reduce nutrient concentrations in effluents.

Water quality models (e.g. Qual2K, WASP, C-RIVE, etc.) constitute efficient integrative tools to study spatio-temporal variations in N dynamics and processes at different degrees of complexity (Raimonet et al., 2015; Wagenschein and Rode, 2008). They can not only quantify the net retention but also assess the retention via two pathways, i.e., assimilatory uptake and denitrification, where the knowledge of relative importance of two pathways and its controlling factors remains partial (Mulholland et al., 2008). Moreover, water quality models are applicable to systems with complex input signals and multiple N species. However, the biggest challenge of using water quality models to offer insights on turnover processes is to constrain the model properly and lower its uncertainty at a reasonable level, since they usually tend to simulate a large number of biogeochemical processes. A Bayesian approach for parameter estimation and uncertainty quantification is regarded as the most adequate procedure for an ‘overparameterized’ model (Janse et al., 2010). Also, it is essential to build on monitoring datasets that include certain spatiotemporal resolutions and scales that are consistent with modeling objectives.

In this study, the direct effects of PS inputs on stream DIN retention capacity and pathways on a typical urban river in Hefei China were investigated under low-flow conditions. To this end, the main investigated river was divided into three reaches: one reference upstream reach, one downstream reach impacted by the untreated wastewater, and one downstream reach dominated by the WWTP effluent (with advanced tertiary treatment). Specifically, our goals of the study were to examine and compare DIN concentrations, assimilatory uptake and

denitrification rates and efficiencies, the relative importance of pathways and its controlling factor, and finally total DIN retention ratios in the 3 representative reaches. We hypothesized that the untreated wastewater would lower both the instream assimilatory uptake rate and efficiency, while the WWTP effluent would elevate both the denitrification rate and efficiency. We also hypothesized that the relative importance of pathways would be regulated by stream metabolism. Finally, we hypothesized that the high loadings from the untreated wastewater input would impair the total DIN capacity in receiving waters, while the WWTP effluent discharge would enhance it.

## **2. Material and Methods**

### *2.1. Study area*

The Nanfei River has a total length of approximately 70 km, flows through Hefei City and enters Chaohu Lake, which is the fifth largest freshwater lake in China and suffers severe algal blooms. The entire catchment area is approximately 1527 km<sup>2</sup>. The annual mean air temperature and precipitation is 15.7 °C and 964 mm, respectively (Hefei Bureau of Statistics, 2018). Hefei is one of the most rapidly urbanized and populated cities in China. Over the past ten years, the population of Hefei City increased by 55% from 2007 to 2017 (reaching 7.42 million), and the gross domestic product increased by 400% from 2007 to 2017 (reaching ¥700 billion) (Hefei Bureau of Statistics, 2018). However, one of the side effects of this fast growth is that the Nanfei River not only faces increasing water scarcity due to the extensive water consumption of the growing population but also experiences heavy pollution because it receives a large amount of PS inputs from the city (Huang et al., 2016).

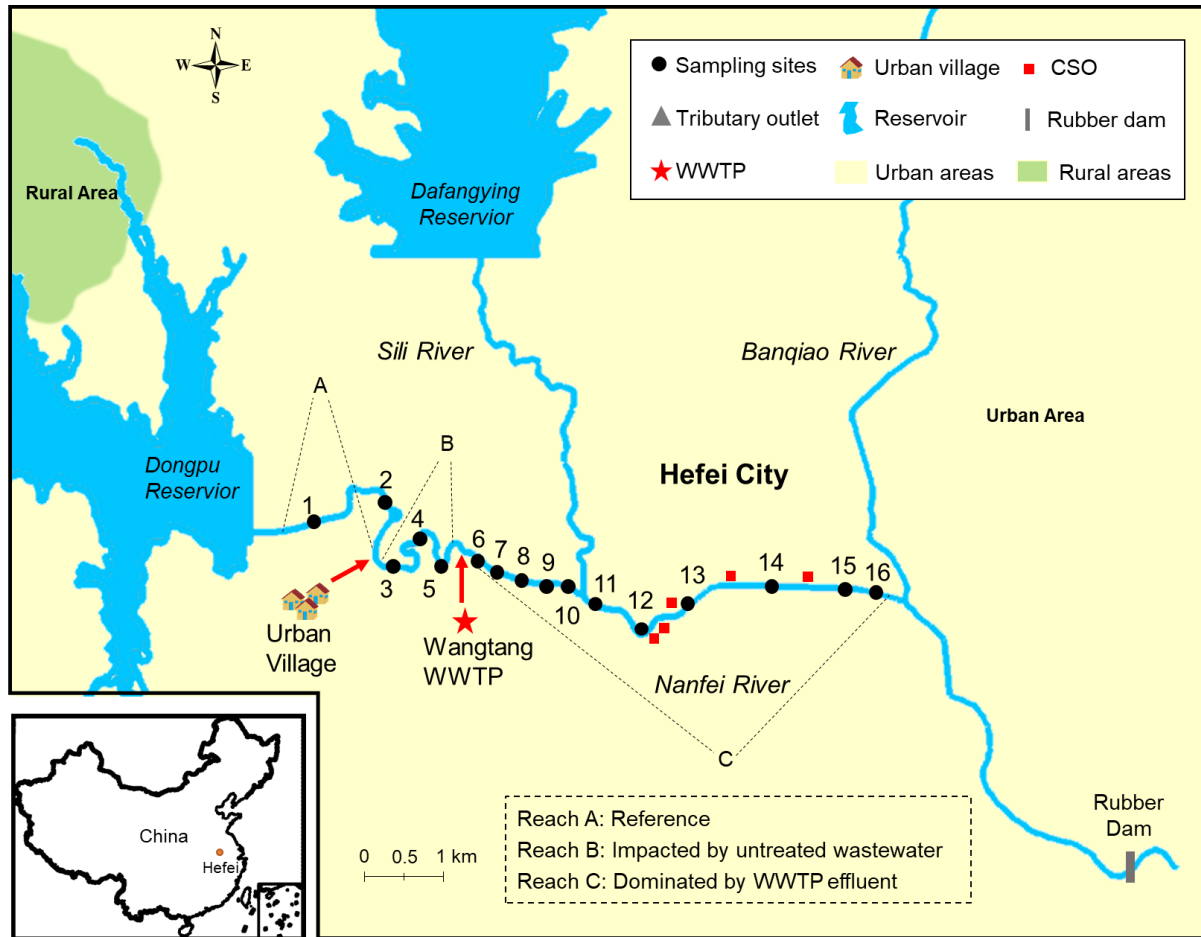


**Figure 1** Nanfei River system, land use and sampling sites in Hefei City, China. The black dots denote the 16 sampling sites. The red squares refer to combined sewer overflow (CSO) locations. The main reach was divided into three sections: reach A (contains Sites 1-2), reach B (Sites 3-5) and reach C (Sites 6-16), which refer to upstream reference reach, wastewater-impacted reach and effluent-dominated reach, respectively.

This study focuses on the central urban section of Nanfei River from the Dongpu Reservoir outlet to the reach approximately 11 km downstream (Figure 1). Two drinking water reservoirs intercept all clean upland water to provide a safe drinking water supply for Hefei only except flooding period, which disconnects the continuity of the urban section from its upstream.

An urban village is located ~2.5 km downstream from the Dongpu Reservoir (between Sites 2 and 3, Figure 1), and this village directly discharges untreated wastewater from a collection pond

through a drain into the river. The Wangtang WWTP is located ~5 km downstream from the reservoir (at Site 6, Figure 1) and treats 200,000 m<sup>3</sup> wastewater per day. The Wangtang WWTP adopts advanced tertiary treatment process using an oxidation ditch with a nitrification/denitrification unit that removes up to 80% of N from the influent. The effluent accounts for ~60% and ~75% of the discharge (gauging station at Site 14) for the whole year and for low-flow periods, respectively (Huang et al., 2016). To maintain river depth in the urban section, a rubber dam is installed and manipulated at ~17 km (Figure 1), which results in low velocity and long travel time of the whole section. Since the water depth is artificially controlled and the main flow contributions from PSs are steady, the hydrodynamics of the river are relatively stable throughout the year except during large rain events, when the combined sewer system can overflow at many points (Figure 1). The river's 2015 hydrograph at Site 14 is presented in supporting information (Figure S1). In addition, the water quality of the urban section was found in our previous study to be mostly determined by the PS discharges, and spatially clustered into the reference Reach A, the wastewater-impacted Reach B, and effluent-dominated Reach C (Figure 1) (Huang et al., 2018). Thus, the Nanfei River provides an ideal experimental system for offering insight into the impacts of PS discharges on the DIN retention under low-flow conditions.

## *2.2. Hydrological and water quality data*

The morphological properties of the studied river section are well documented (Internal Material). The riverbed morphology of the studied reach was surveyed by a governmental agency and characterized by 262 cross-sections. Daily water stage data are available from the gauge station at Site 14 (Figure 1). Daily discharge data of the reservoir water release, WWTP effluent, and combined sewer overflow (CSO) from pumping stations were obtained from the Hefei Urban

Drainage Management Authority (HUDMA). The daily discharge of untreated wastewater was assumed constant and determined based on the number of inhabitants in the urban village and the sewage-discharge equivalent per capita (MOHURD China, 2014). Monthly water quality data during April till November 2015 (Period I, Table 1) were made available by HUDMA. Ammonium ( $\text{NH}_4^+$ ), nitrate ( $\text{NO}_3^-$ ), total nitrogen (TN), dissolved oxygen (DO), biological oxygen demand (BOD), and total phosphorus (TP) were routinely monitored at Sites 2, 5, 8, 12, 13, 14 and 15 and Sili River outlet. The concentrations of 5 CSO effluents were described by the values of the event mean concentrations (EMCs) from the same pumping stations (Li et al., 2014).

**Table 1** Information of tow sampling and modeling periods.

Name	Sampling/Modeling Period	Sampling Frequency	No. of Sites	No. of Constituents	Use of Data
I	01/04/2015-05/11/2015	Monthly	7	6	Validation
II	03/10/2015-06/10/2015	Bi-hourly	16	13	Calibration

To complete the database and to gain an overview of water quality with higher longitudinal resolution, a hydrological and water quality survey was intensively conducted under low-flow conditions in October 2015 (Period II, Table 1). Diurnal variations were recorded by collecting bihourly samples from the 16 selected study sites as well as from the urban village, WWTP effluent and Sili River outlet. The water quality parameters included temperature, pH, DO, chlorine (Cl), chlorophyll-a (Chl-a),  $\text{NH}_4^+$ ,  $\text{NO}_3^-$ , dissolved organic nitrogen (DON), TN, dissolved organic carbon (DOC), phosphate, and TP. Details of hydrological survey, sampling methods and chemical analyses could be referred to our previous study (Huang et al., 2017).

### 2.3. Model setup

The hydrodynamic model was prepared using the software EPDRiv1 (NRE, 2014), and the biogeochemical transformations affecting DIN concentrations (Figure S2 and Table 2) of the Nanfei River was simulated with the EUTRO module of WASP 7.5.2. (Wool et al., 2002).

**Table 2** The rate of change in mass flux ( $S_k$ , in  $\text{mg N L}^{-1} \text{d}^{-1}$ ) of the biogeochemical processes related to DIN cycling in the WASP model\*.

Process	Notation	$\text{NH}_4^+$	$\text{NO}_3^-$
<b>Nitrification</b>	NIT	$-k_{12}E_{12}^{T-20}\left(\frac{C_6}{K_{\text{NIT}} + C_6}\right)C_1$	$k_{12}E_{12}^{T-20}\left(\frac{C_6}{K_{\text{NIT}} + C_6}\right)C_1$
<b>Denitrification</b>	DEN		$-k_{2D}E_{2D}^{T-20}\left(\frac{K_{\text{NO}_3}}{K_{\text{NO}_3} + C_6}\right)C_2$
<b>Mineralization</b>	MIN	$k_{71}E_{71}^{T-20}\left(\frac{C_4}{K_{\text{mC}} + C_4}\right)C_7$	
<b>Phytoplankton Death Release</b>	R	$D_{p1}a_{\text{NC}}(1 - f_{\text{ON}})C_4$	
<b>Phytoplankton Assimilatory Uptake</b>	A	$-G_{p1}a_{\text{NC}}P_{\text{NH}_3}C_4$	$-G_{p1}a_{\text{NC}}(1 - P_{\text{NH}_3})C_4$

\* Notations of the model parameters are shown in Table 3. C1, C2, C4, C6 and C7 represent the concentrations of  $\text{NH}_4^+$ ,  $\text{NO}_3^-$ , phytoplankton biomass carbon, DO and DON, respectively

The model domain started at the reservoir outlet and ended at the confluence with the Banqiao River (Figure 1). The entire reach was divided into 45 model segments, each with an average length of about 200 m. For the setup of EPDRiv1 model, the geometric information of each segment was generated using the data of cross-sectional profiles. For hydrodynamic modeling, the discharge of water released from the reservoir defined the upper boundary. The inflows of the Sili River and urban village, which were small compared to the main stream flow, were assumed to be constant. The discharges of WWTP effluent and CSOs were inputted at a daily time step to the model with the provided data. The hydrodynamic model was directly set up for

Period I for validation, using the Manning friction coefficient from the model calibration in our previous study (Huang et al., 2017).

For the WASP model, the upper boundary condition was forced by the reservoir water quality data. The lateral boundary condition of urban village was described constantly with the data from the intensive survey. The lateral boundary conditions of the WWTP effluent, Sili River, and CSOs were defined at a daily time step by interpolation of monthly data or averaging of bi-hourly data. The WASP model was firstly set up for Period II and run until reaching a steady-state condition. By taking full account of the instream longitudinal variations of constituents under low-flow conditions, parameter sensitivity analysis, automatic calibration and uncertainty analysis were conducted with this setup. Then the model was set up and run dynamically for Period I for validation. The time step for each run was calculated by WASP to ensure the numerical stability.

#### *2.4. Parameter identification and uncertainty analysis*

For the validation of the hydrodynamic model, the goodness-of-fit of the simulated water level at Site 14 was evaluated by three performance criteria, namely Nash-Sutcliffe -Efficiency (NSE) coefficient, Root Mean Square Error (RMSE) and Percent BIAS (PBIAS). The identification of complex water quality model was comprised of three steps.

- a. Sensitivity Analysis* This step aims at screening the most influential parameters. 23 parameters related to the N processes were chosen (Table 3). The parameter distribution was defined uniformly within the ranges reported in literatures (Bowie et al., 1985; Wool et al., 2002). The Elementary Effects (EE) method (Morris method) was selected and the analysis were performed using the SAFE toolbox (Pianosi et al., 2015). Considering the system in its entirety, the objective function was firstly defined by the mean of NSE

coefficients of  $\text{NH}_4^+$ ,  $\text{NO}_3^-$ , DON, Chl-a and DO. Then, the objective functions were defined respectively by the NSE of  $\text{NH}_4^+$ ,  $\text{NO}_3^-$  and DON to identify the parameters which are globally less sensitive, but locally sensitive for a single N variable.

*b. Automatic-calibration* After the sensitivity analysis, the most identifiable parameters were used for model calibration based on the Gauss–Marquardt–Levenberg algorithm with OSTRICH v17.12.19. (Matott, 2005). The ranges of the selected parameters were defined the same as in the sensitivity analysis (Table 3). The objective function was defined by the weighed sum of square error of five variables ( $\text{NH}_4^+$ ,  $\text{NO}_3^-$ , DON, Chl-a and DO) using 80 measurements from averaged bi-hourly observations at each site. All other less sensitive parameters were set according to values obtained from manual calibration from our previous stud (Huang et al., 2017).

*c. Model validation* NSE, RMSE and PBIAS were used to evaluate the model performance of the 6 water quality variables from Period I.

**Table 3** Stoichiometry and kinetic parameters related to N processes in the WASP model.

Parameter	Notation	Unit	Optimal value	Literature values <sup>a</sup>
Nitrification rate constant at 20 °C	$k_{12}$	$\text{d}^{-1}$	0.11	0.09-0.13 (A)
Half-saturation constant for nitrification oxygen limit	$K_{\text{NIT}}$	$\text{mg O L}^{-1}$	1.10	0-2 (A)
Denitrification rate constant at 20 °C	$k_{2D}$	$\text{d}^{-1}$	0.97	0-1 (B)
Half-saturation constant for denitrification oxygen limit	$K_{\text{NO}_3}$	$\text{mg O L}^{-1}$	0.09	0-1.5 (A)
Phytoplankton maximum growth rate constant at 20 °C	$k_{1c}$	$\text{d}^{-1}$	2.98	0-3 (A)
Phytoplankton growth temperature coefficient	$E_{1C}$	--	1.07	1-1.07 (A)
Phytoplankton death rate constant	$k_{1D}$	$\text{d}^{-1}$	0.30	0-1 (B)
Phytoplankton nitrogen to carbon ratio	$a_{\text{NC}}$	--	0.25	0.05-0.43 (B)
Phytoplankton phosphorus to carbon ratio	$a_{\text{PC}}$	--	0.045	0.0024-0.24 (B)
Fraction of algal death that recycles to ON	$f_{\text{ON}}$	--	0.97	0-1 (A)

Fraction of algal death that recycles to OP	$f_{OP}$	--	0.5	0-1 (A)
Nitrification temperature coefficient	$E_{12}$	--	1.045	1-1.07 (A)
Denitrification temperature coefficient	$E_{2D}$	--	1.045	1-1.045 (A)
ON mineralization rate constant at 20°C	$k_{71}$	$d^{-1}$	0.08	0.02-0.1 (B)
ON mineralization temperature coefficient	$E_{71}$	--	1.045	1.02-1.09 (B)
Phytoplankton endogenous respiration rate constant	$k_{1R}$	$d^{-1}$	0.125	0.05-0.2 (B)
Phytoplankton respiration temperature coefficient	$E_{1R}$	--	1.045	1-1.07 (B)
Half-Saturation constant for nitrogen	$K_{mN}$	$mg\ N\ L^{-1}$	0.015	0-0.05 (A)
Half-Saturation constant for phosphorus	$K_{mP}$	$mg\ P\ L^{-1}$	0.02	0.0005-0.03 (A)
Half-saturation constant for phytoplankton limitation in nitrogen recycle	$K_{mC}$	$mg\ C\ L^{-1}$	0.8	0-1 (A)
Saturating light intensity	$I_s$	$Langley\ d^{-1}$	250	200-500 (A)
Phytoplankton carbon to chlorophyll ratio	$E'_c$	--	50	20-100 (B)
OP mineralization rate constant at 20°C	$k_{83}$	$d^{-1}$	0.1	0.01-0.22 (A)
Phytoplankton growth rate constant	$G_{pl}$	$d^{-1}$	$k_{1c} X_{RT} X_{RI} X_{RN}^c$	
Phytoplankton death rate constant	$D_{pl}$	$d^{-1}$	$k_{1R} E_{1R}^{(T-20)} + k_{1D}^d$	
Preference for ammonia uptake term <sup>e</sup>	$P_{NH3}$	--	$C_1 \left( \frac{C_2}{(K_{mN} + C_1)(K_{mN} + C_2)} \right) + C_1 \left( \frac{K_{mN}}{(C_1 + C_2)(K_{mN} + C_2)} \right)$	

<sup>a</sup> Sources of literature values: (A) Wool et al. (2002); (B) Bowie et al. (1985).

<sup>b</sup> The upper-most 11 parameters are the most identifiable ones used for auto-calibration and uncertainty analysis.

<sup>c</sup>  $X_{RT}$ ,  $X_{RI}$  and  $X_{RN}$  refers to dimensionless temperature adjustment factor, light and nutrient limitation factor, respectively.

<sup>d</sup>  $T$  represents water temperature.

<sup>e</sup> More details on the calculation of  $G_{pl}$ ,  $D_{pl}$  and  $P_{NH3}$  are provided in the WASP manual

A widely used Markov Chain Monte Carlo (MCMC) approach was also integrated to evaluate model uncertainties using DREAM (Vrugt, 2016). Simulations were performed with the uniform prior distributions of parameters for the same ranges as used in the automatic-calibration. Model parameter inferences were based on the log-likelihood function:

$$\log L = -\frac{M}{2} \log(2\pi) - \sum_{i=1}^M \log \sigma_i - \frac{1}{2} \sum_{i=1}^M \frac{1}{\sigma_i^2} (C_i^{obs} - C_i^{sim})^2 \quad (1)$$

where  $i$  and  $M$  donate the  $i^{th}$  measurement and the number of measurements, respectively;  $C^{obs}$  and  $C^{sim}$  are log10-transformed observed and simulated concentrations of five variables ( $NH_4^+$ ,  $NO_3^-$ , DON, DO and Chl-a) respectively;  $\sigma$  denotes standard deviation of the Gaussian distribution of  $C^{obs}$ . In our case common  $\sigma$  is assumed for  $NH_4^+$ ,  $NO_3^-$ , DON, DO and Chl-a individual

observations, respectively. These five standard deviations are included in the set of parameters estimated in the MCMC simulation. The 95% confidence band of parameter uncertainty was generated from 64,000 MCMC evaluations.

## 2.5. DIN uptake metrics and retention ratio

DIN uptake metrics, including denitrification rate and velocity ( $U_{DEN}$ ,  $v_{f,DEN}$ ), the assimilatory  $\text{NH}_4^+$  uptake rate and velocity ( $U_{A-NH4}$ ,  $v_{f,A-NH4}$ ), and the assimilatory  $\text{NO}_3^-$  uptake rate and velocity ( $U_{A-NO3}$ ,  $v_{f,A-NO3}$ ) were calculated in each segment, respectively. They were calculated based on the rate of change in mass flux for each process (Table 2) with the equations below:

$$U = S_K \times z \quad (2)$$

$$v_f = \frac{U}{c} \quad (3)$$

where  $U$  is aerial uptake rate (mass per unit area of streambed per unit time,  $\text{g m}^{-2} \text{d}^{-1}$ ) and  $v_f$  for uptake velocity (a measure of uptake efficiency relative to availability,  $\text{cm s}^{-1}$ ),  $z$  is the depth (m), and  $c$  is the simulated  $\text{NH}_4^+$  or  $\text{NO}_3^-$  concentration ( $\text{mg N L}^{-1}$ ). The relative importance of two processing pathways, namely assimilatory uptake and denitrification, was calculated as  $v_{f,A} / v_{f,DEN}$ . DIN budgets were derived from the model outputs from the intensive survey in Period II. For each segment  $i$ , mass balance of  $\text{NH}_4^+$  or  $\text{NO}_3^-$  can be written as:

$$\frac{\partial c_i V_i}{\partial t} = S_{Adv,i} V_i + S_{Disp,i} V_i + S_{L,i} V_i + S_{B,i} V_i + S_{K,i} V_i \quad (4)$$

where the equation accounts for all the material entering and leaving through advective and dispersive transport (terms 1 and 2), direct loading (term 3), boundary condition (term 4), and physical, chemical, and biological transformation (term 5). The differential form of equation 4 for a steady-state simulation can be written as:

$$0 = Q_{i-1,i}c_{i-1,i} - Q_{i,i+1}c_{i,i+1} + E'_{i-1,i}(c_{i-1} - c_i) + E'_{i,i+1}(c_{i+1} - c_i) + S_{L,i}V_i + S_{B,i}V_i + S_{K,i}V_i \quad (5)$$

247 where  $Q$ ,  $c$ ,  $E'$  and  $V$  refer to flow, concentration, dispersion coefficient and volume, respectively;  
 248 double-subscripted terms refer to the interfaces between segments.

249 The transformation term ( $S_K$ ) of  $\text{NH}_4^+$  and  $\text{NO}_3^-$  in each segment could be expressed as:

$$S_{K-\text{NH}_4^+} = -S_{K-\text{NIT}} + S_{K-\text{MIN}} + S_{K-\text{R}-\text{NH}_4^+} - S_{K-\text{A}-\text{NH}_4^+} \quad (6)$$

$$S_{K-\text{NO}_3^-} = S_{K-\text{NIT}} - S_{K-\text{DEN}} - S_{K-\text{A}-\text{NO}_3^-} \quad (7)$$

250 The calculation of each biogeochemical process could be referred to the formula in Table 2. The  
 251 parameter values were taken from the model identification, and the concentrations were given  
 252 by the simulation results in each segment.

253 The mass fluxes ( $\text{kg N d}^{-1}$ ) were integrated over the three river domains (i.e., Reaches A, B and C;  
 254 Figure 1). The DIN retention ratios and pathway ratios of the three representative reaches were  
 255 calculated as:

$$RR = \frac{S_{K-U} + S_{K-DEN}}{S_{Adv} + S_{Disp} + S_L + S_B} \times 100\% \quad (8)$$

$$RR_L = \frac{RR_{DIN}}{Length} \quad (9)$$

$$PR_A = \frac{S_{K-U}}{S_{K-U} + S_{K-DEN}} \times 100\% \quad (10)$$

$$PR_{DEN} = \frac{S_{K-DEN}}{S_{K-U} + S_{K-DEN}} \times 100\% \quad (11)$$

256 where  $RR$  (%) is the total DIN retention ratio,  $PR_A$  (%) and  $PR_{DEN}$  (%) are the share of assimilatory  
 257 uptake and denitrification on total DIN retention respectively. In order to compare the DIN

retention capacities in the three reaches and with other studies, the DIN retention ratio was normalized by the distance of each reach, noted by  $RR_L$  (% km<sup>-1</sup>).

### 3. Results

#### 3.1. Model calibration and validation

The hydrodynamic model adequately reproduced manipulated water level (by rubber dam station) at low-flow and the influence of CSOs at high-flow (Figure S3). Statistically, an NSE of 0.92, a PBIAS of -0.01% and an RMSE of 0.11 m confirmed the good agreement between simulated and measured values. The longitudinal discharge graph provides a systematic overview of the flow composition under low-flow conditions (Figure 2a). Reach A received a small inflow (0.1 m<sup>3</sup> s<sup>-1</sup>) due to the upstream interception of reservoir. The untreated wastewater from urban village contributed 50% of the discharge in Reach B, while the WWTP effluent dominated the discharge in Reach C (>70%).

The parameter sensitivity ranking showed the parameters that control phytoplankton growth, including  $k_{1c}$ ,  $k_{1D}$ ,  $a_{PC}$ ,  $f_{OP}$  and  $E_{1c}$ , influenced globally the goodness-of-fit the most (Figure S4). Besides, six other locally sensitive parameters including  $k_{12}$ ,  $K_{NIT}$ ,  $k_{2D}$ ,  $K_{NO3}$ ,  $f_{ON}$  and  $a_{NC}$  were added to the identifiable parameters (Figure S4).

The best-fitting model parameters from automatic calibration results are presented in Table 3. The simulated and measured values of Chl-a, DO, DON, NH<sub>4</sub><sup>+</sup> and NO<sub>3</sub><sup>-</sup> reproduced the variables significantly well (Figure 2). The simulation results of Cl, DOC, DIP, and TP also supported the good model performance (Figure S6). The objective criteria NSE of the three N variables were higher than 0.85 for the calibrated model (Table 4), reflecting the capability of the model to represent the N variations well. The simulated values for NH<sub>4</sub><sup>+</sup> had larger errors than did those for

NO<sub>3</sub><sup>-</sup> and DON (Table 4). This can be explained by the fact that the simulated NH<sub>4</sub><sup>+</sup> values at Sites 4 and 5 had a large deviation from the measured ones (Figure 2e).

**Table 4** Model calibration and validation performance expressed by NSE, PBIAS and RMSE.

<b>Calibration</b>										
<b>Criterion</b>	<b>Unit</b>	<b>NH<sub>4</sub><sup>+</sup></b>	<b>NO<sub>3</sub><sup>-</sup></b>	<b>DON</b>	<b>Chl-a</b>	<b>DO</b>	<b>DIP</b>	<b>TP</b>	<b>DOC</b>	<b>CI</b>
NSE	--	0.87	0.99	0.93	0.97	0.97	0.65	0.76	0.53	0.99
PBIAS	%	-20.36	-0.72	4.31	7.03	3.65	-1.45	5.21	12.41	0.95
RMSE*	mg L <sup>-1</sup>	0.89	0.33	0.10	9.44	0.51	0.09	0.06	1.00	1.81
<b>Validation</b>										
<b>Criterion</b>	<b>Unit</b>	<b>NH<sub>4</sub><sup>+</sup></b>	<b>NO<sub>3</sub><sup>-</sup></b>	<b>TN</b>	<b>DO</b>	<b>TP</b>	<b>BOD<sub>5</sub></b>			
NSE	--	0.96	0.88	0.97	0.93	0.94	0.85			
PBIAS	%	-3.99	-3.65	2.48	5.40	6.17	5.50			
RMSE*	mg L <sup>-1</sup>	0.81	0.90	0.86	1.15	0.12	2.10			

\*The unit of Chl-a RMSE is in µg L<sup>-1</sup>.

For validation, the water quality results were compared with the data from the routine sampling program from the authority. The NSE of NH<sub>4</sub><sup>+</sup> and NO<sub>3</sub><sup>-</sup> were higher than 0.85. Large deviations occurred in the values of NH<sub>4</sub><sup>+</sup> and NO<sub>3</sub><sup>-</sup> (Figure S5), which could be mainly attributed to the impacts of several CSOs during the validation period. Other measured variables (including TN, TP, DO and BOD) were also well reproduced in the validation (Figure S5 and Table 4). Notably, supersaturated DO levels consistently occurred at Site 2, except for the samplings on 01.07.2015 and 29.07.2015. These results support the consistent algal bloom and the high primary productivity observed at Site 2 during the intensively-monitoring period.

The uncertainties of most water quality variables in the upstream of WWTP effluent were much higher than those downstream, demonstrating that the highly nonlinear processes would lead to higher uncertainty in the model domain of a more eutrophic system like upstream (Figure 2b). The 95% parameter uncertainty band covered most observations. The Chl-a and DO simulations in the upstream and NO<sub>3</sub><sup>-</sup> simulations in the downstream were close to the parameter uncertainty

boundaries, because the optimal values of their most influential process parameters (e.g.,  $k_{1c}$  and  $k_{2b}$ ) are close to the upper boundaries of the parameter value ranges (Table 3).

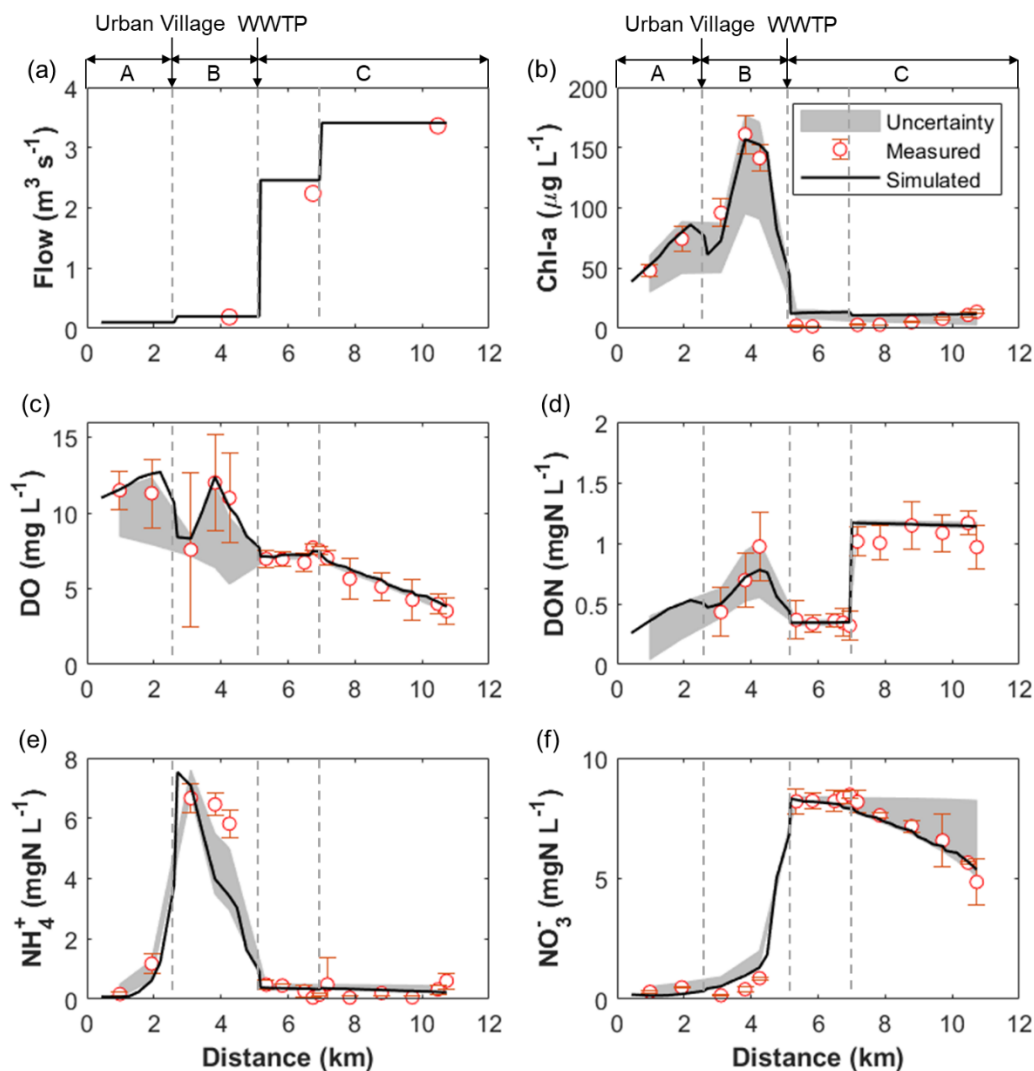


**Figure 2** Longitudinal measured and simulated (a) discharge and concentrations of (b) Chl-a, (c) DO, (d) DON, (e)  $\text{NH}_4^+$ , and (f)  $\text{NO}_3^-$  at low flow in the Nanfei River. The 95% confidence band of parameter uncertainty is depicted in grey. The error bar shows the standard deviation of bi-hourly data.

### 3.2. Longitudinal DIN variations

The concentration of  $\text{NH}_4^+$  at Site 1 was less than  $0.2 \text{ mg N L}^{-1}$  (Figure 2e), and this value represented the background level of  $\text{NH}_4^+$  in the reference Reach A. At Site 3, the untreated

wastewater discharged from the urban village significantly raised the  $\text{NH}_4^+$  concentration to more than  $7 \text{ mg N L}^{-1}$ . In the following Reach B, the  $\text{NH}_4^+$  level declined. Meanwhile, the Chl-a, as a proxy of phytoplankton biomass, peaked at approximately  $160 \mu\text{g L}^{-1}$  (Figure 2b), which would explain the  $\text{NH}_4^+$  decrease via assimilatory uptake in this reach. However, the concentration of  $\text{NH}_4^+$  at Site 6 abruptly dropped due to its lower concentration in the effluent discharge since it is usually fully processed in the WWTP. Downstream from WWTP in Reach C, the ambient  $\text{NH}_4^+$  levels remained low, with few changes ( $0.05\text{-}0.61 \text{ mg N L}^{-1}$ , Figure 2e).

In Reach A, the concentrations of  $\text{NO}_3^-$  measured at the most upstream sites were less than  $1 \text{ mg N L}^{-1}$  (Figure 2f). With the discharge of untreated wastewater at Site 3, the concentration of  $\text{NO}_3^-$  did not change significantly due to the low concentration of  $\text{NO}_3^-$  in the raw sewage ( $0.4 \text{ mg N L}^{-1}$ ). However, it increased in Reach B, which could be attributed to the dispersive inputs from WWTP or transformed from  $\text{NH}_4^+$  via nitrification. In Reach C, the  $\text{NO}_3^-$  concentration significantly elevated with the WWTP effluent discharge at Site 6 (Figure 2f). Even though the treatment processes of the WWTP include a nitrogen removal unit, the  $\text{NO}_3^-$  concentration in the effluent ( $9.0 \text{ mg N L}^{-1}$ ) was still much higher than the ambient concentration. The  $\text{NO}_3^-$  concentrations notably declined between Sites 11 and 16 (Figure 2f), which implied strong removal of  $\text{NO}_3^-$ . Considering the low Chl-a concentrations ( $< 5 \mu\text{g L}^{-1}$ , Figure 2b) in the effluent-dominated section, assimilatory uptake probably played a small role in DIN retention. Furthermore, the hypoxic ambient environment (Figure 2c) might enhance the occurrence of denitrification in Reach C.

### 3.3. DIN uptake metrics

As shown in Figure 3a, the longitudinal  $U_{\text{A-NH}_4}$  variation tendency was consistent with the longitudinal Chl-a level (Figure 2b). The  $U_{\text{A-NH}_4}$  peaked synchronously with the Chl-a concentration

in Reaches A and B. It reached approximately  $2.5 \text{ g N m}^{-2} \text{ d}^{-1}$  at 4 km with algal blooms in reach B. With the discharge of WWTP effluent, the  $U_{A-NH_4}$  dropped below the level of  $0.01 \text{ g N m}^{-2} \text{ d}^{-1}$  and stayed low in Reach C. As shown in Figure 3c, the  $U_{A-NO_3}$  reached the highest level (approximately  $0.12 \text{ g N m}^{-2} \text{ d}^{-1}$ ) at ~2 km in Reach A. The  $U_{A-NO_3}$  experienced a small peak around the location where algal blooms occurred in Reach B. The value ( $0.016 \text{ g N m}^{-2} \text{ d}^{-1}$ ), however, was still far below the  $U_{A-NH_4}$ . In Reach C, the  $U_{A-NO_3}$  level remained low.

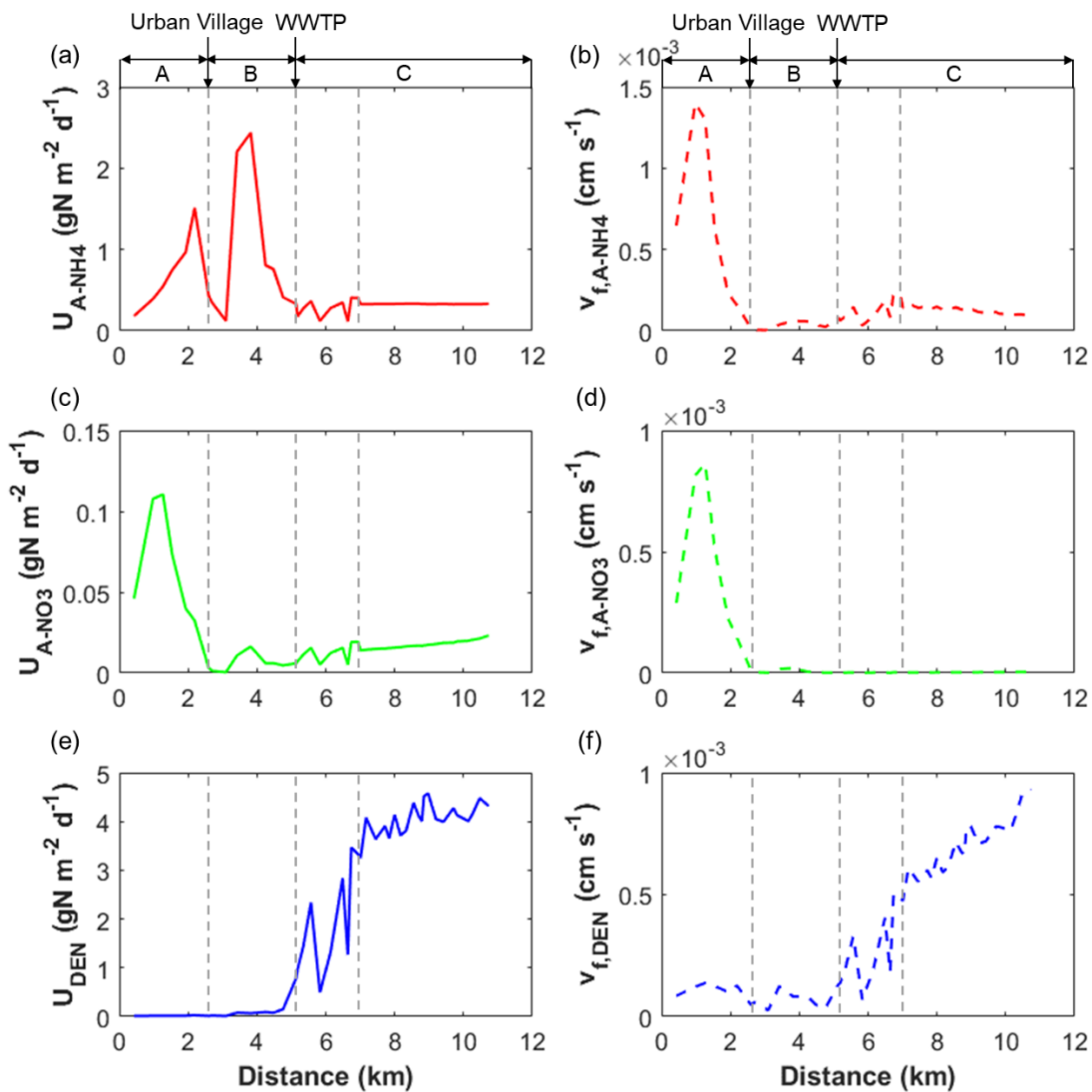


**Figure 3** Longitudinal variations in metrics of DIN uptake in the Nanfei River.

In terms of assimilatory uptake efficiency,  $v_{f,A-NH4}$  was the highest, with a peak value close to  $1.5 \times 10^{-3} \text{ cm s}^{-1}$  at ~2 km in Reach A (Figure 3b). However, with the wastewater discharges,  $v_{f,A-NH4}$  decreased significantly and remained below  $5 \times 10^{-4} \text{ cm s}^{-1}$  in Reaches B and C. The longitudinal variations in  $v_{f,A-NO3}$  had similar trends with those of  $v_{f,A-NH4}$ ; nevertheless, there were significant differences in their numerical values (Figure 3d).

As shown in Figure 3e, the  $U_{DEN}$  values in Reaches A and B were very small. With the WWTP effluent discharge, the  $U_{DEN}$  increased rapidly. Between the two tributaries in Reach C, the  $U_{DEN}$  reached and fluctuated around approximately  $4 \text{ g N m}^{-2} \text{ d}^{-1}$ . The  $v_{f,DEN}$  had similar longitudinal variation trends as  $U_{DEN}$  (Figure 3f). The  $v_{f,DEN}$  remained low in Reaches A and B, though it increased with distance in Reach C.

#### 3.4. DIN retention ratio

DIN mass balance, retention ratios and pathways are given in Table S1, Figure S7 and Table 5. The total DIN  $RR_L$  in the three reaches ranked as Reach A higher than Reach B higher than Reach C (Table 5). The  $RR_L$  value in Reach A was close to those in Sugar Creek under summer low flow and DIN concentration conditions ( $>20\% \text{ km}^{-1}$ ), while that in Reach C was only similar to those during months of high discharge and DIN concentration in Sugar Creek (Alexander et al., 2009). This result indicated the instream DIN retention capacity was impaired by the influence of the untreated wastewater discharge; and it was further impaired by high DIN loading discharge of the WWTP effluent. In addition, the DIN was mostly retained mainly via assimilatory uptake in both Reaches A and B (Table 5). In contrast, The DIN was mostly removed via denitrification in Reach C (Table 5), which received a large amount of DIN loading mainly in the form of  $\text{NO}_3^-$  (Figure S7). Our results suggested that the different PS inputs could have different effects on the relative

importance of instream DIN retention pathway; however, both led to the same result of decreases in retention capacity.

**Table 5** DIN retention capacities (% km<sup>-1</sup>) and pathways (%) in the three representative reaches.

	Reach A	Reach B	Reach C
$RR_L$ (% km <sup>-1</sup> )	30.3	14.3	6.5
$PR_A$ (%)	99.6	92.0	9.1
$PR_{DEN}$ (%)	0.4	8.0	90.9

## 4. Discussion

### 4.1. Effects of PS inputs on assimilatory uptake rate and efficiency

The instream assimilatory uptake rate and efficiency reacted differently to the two PS inputs in the Nanfei River. The  $U_{A-NH_4}$  was elevated with the untreated wastewater discharge in Reach B as expected, while  $U_{A-NO_3}$  was not. The concentrations of both  $NH_4^+$  and  $NO_3^-$  in Reach A were the lowest in the entire river. Therefore,  $NO_3^-$  was also largely utilized for phytoplankton growth in Reach A because of the insufficient DIN supply here, although  $NH_4^+$  is a preferred DIN substrate for algae due to the lower energy required for its assimilation into biomass (Tank et al., 2017). With the nutrient inputs from the untreated wastewater, the elevated nutrient concentrations stimulated the algal bloom observed in Reach B. Since  $NH_4^+$  was the more abundant and preferred compound, the  $U_{A-NH_4}$  synchronously peaked with the occurrence of the algal bloom. In contrast, the  $U_{A-NO_3}$  in Reach B were lower than that in Reach A because Reach B had adequate  $NH_4^+$  that could be utilized. Despite the elevated rate, the  $v_{f,A-NH_4}$  was diminished in Reach B. In Reach A, phytoplankton growth was restricted by low nutrient concentrations. With the increased nutrient concentrations in Reach B, the assimilatory processes shifted to become restricted by other factors, e.g., light availability (Tank et al., 2017). Therefore, the assimilatory DIN uptake efficiency

declined as nutrient concentrations increased because of the discharge of untreated wastewater in Reach B. Our findings were consistent with the conclusions of elevated assimilatory uptake rate but diminished efficiency attributable to wastewater discharge in previous studies (Gibson and Meyer, 2007; Haggard et al., 2005).

In contrast, our results showed that the WWTP effluent discharge lowered both the assimilatory uptake rate and efficiency in Reach C. Below the WWTP effluent discharge, the total DIN concentrations were still high, with increased  $\text{NO}_3^-$  concentrations and decreased  $\text{NH}_4^+$  concentrations. Due to the dominance of effluent containing negligible phytoplankton biomass, the concentration of Chl-a was strongly diluted in Reach C. Despite the sufficient nutrients and light availability, the recovery of the phytoplankton biomass could not compensate for the impacts of the effluent. Thus, the Chl-a concentrations remained low for several kilometers downstream. Therefore, compared with the assimilatory DIN uptake rates in Reaches A and B, the rates in Reach C were the lowest. In addition, the assimilatory DIN uptake efficiency was even lower, as a result of the higher DIN concentrations and the lower uptake rates. In this case, the huge system shock by the dominant discharge from WWTP diminished both the assimilatory uptake rate and efficiency in the receiving water.

#### *4.2. Impacts of Tertiary WWTP effluent on denitrification rate and efficiency*

Our results showed that both the denitrification rate and efficiency were significantly elevated downstream of the WWTP effluent discharge, which was also reported in the studies by Gucker et al. (2006) and Rahm and et al. (2016). In these two studies and our study, the WWTPs all adopted advanced tertiary treatment process with an N removal unit and their effluents were all  $\text{NO}_3^-$ -dominated.

Other previous studies reported the decline in denitrification efficiency with the increase in  $\text{NO}_3^-$  concentration (Bernot and Dodds, 2005), and there are usually three possible explanations: (i) saturation of benthic microbial nutrient demand, (ii)  $\text{NO}_3^-$  transport rate limitations, and (iii) carbon source supply (Mulholland et al., 2008; Seitzinger et al., 2006). First, denitrification is a microbial process most often occurring in anoxic zones. With abundant oxygen in the water column, the likelihood of the denitrification process occurring in the overlying water is limited. If denitrification occurs mostly in the sediments, high DIN concentrations in the water column may exceed or saturate the nutrient demand of the benthic microbial community (Bernot and Dodds, 2005). Second, with abundant oxygen in the water column, the uppermost sediment will be maintained at a high redox level. As denitrification occurs below this oxidized zone, a longer diffusion pathway for  $\text{NO}_3^-$  will limit the denitrification rate despite the abundant existence of  $\text{NO}_3^-$  in the water column (Seitzinger et al., 2006). Third, denitrification, as classically defined, is a heterotrophic process that utilizes organic carbon as an electron donor. In some cases, the denitrification rate can reach saturation with increasing  $\text{NO}_3^-$  concentrations due to the limited supply of carbon (Figuerola-Nieves et al., 2015).

However, none of these three explanations applied to Reach C, which was dominated by WWTP effluent. In Reach C, there was a longitudinal gradient of DO depletion, and the hypoxic environment in the overlying water provided favorable conditions for denitrification, which meant denitrification was no longer confined to the sediments. In contrast to those cases in which diffusion dominated the transport of  $\text{NO}_3^-$  between the sediment-water interface, the  $\text{NO}_3^-$ -rich aerobic water was delivered into a region of sub-oxic water through longitudinal advection in Reach C. In these advection-dominated systems,  $\text{NO}_3^-$  can be continuously

denitrified within the water column when it is sub-oxic. Additionally, it has been suggested the N biotic demand increases with increases in river size; this is caused by the contribution of the water column processes in addition to the benthic dynamics (David et al., 2011). The simultaneous demand by both benthic and water column biotic processes will impede the occurrence of N retention saturation. In addition, Rahm et al. (2016) provided evidence that, after tertiary treatment, WWTP effluent contained enriched denitrifying communities relative to those in the ambient stream water; this was determined by measuring the functional genes associated with denitrification. Though we do not have direct evidence of a shift in the microbial community in response to the WWTP effluent, it is inferred that the denitrifying bacteria discharged from the WWTP may inoculate river microbial communities and influence the dominance of the effluent observed in Reach C. Moreover, the WWTP effluent contributes to both  $\text{NO}_3^-$  and organic matter loadings. The adequate DOC supply prevented N retention saturation due to the lack of a carbon source in Reach C. Therefore, both the denitrification rate and efficiency were elevated in the effluent-dominated Reach C of Nanfei River. Our study provides evidence that the advanced tertiary WWTP may not necessarily lead to diminished denitrification rate and efficiency in receiving waters.

#### *4.3. Relationships between DIN retention pathways and metabolism*

Assimilatory uptake and denitrification accounted for instream DIN retention. The relative importance of these processes as well as the mechanisms involved gain increasing research interest (Mulholland et al., 2008). The results of our previous study demonstrated that the ratios of areal rate of system primary production to respiration (P/R) were close to 1 in Reach A (Figure S8) (Huang et al., 2017). After receiving the untreated wastewater with inputs of nutrients and

organic matter, both the heterotrophic and the autotrophic activity rates were enhanced. Nevertheless, primary production outpaced respiration, with P/R ratios higher than 1 in Reach B; as a result, the system shifted to net autotrophy. However, the ecosystem became net heterotrophic, with P/R ratios lower than 0.5, in Reach C. In this study, our data suggested that the relative importance of assimilatory uptake and denitrification (presented as  $v_{f,A} / v_{f,DEN}$ ) was positively related with the P/R ratio ( $R^2 = 0.61$ ,  $p < 0.05$ , Figure 4), indicating that autotrophy enhanced assimilatory uptake and heterotrophy enhanced denitrification. These results verified our hypothesis that the metabolism continued regulating DIN uptake pathways in stream impacted by PS inputs.

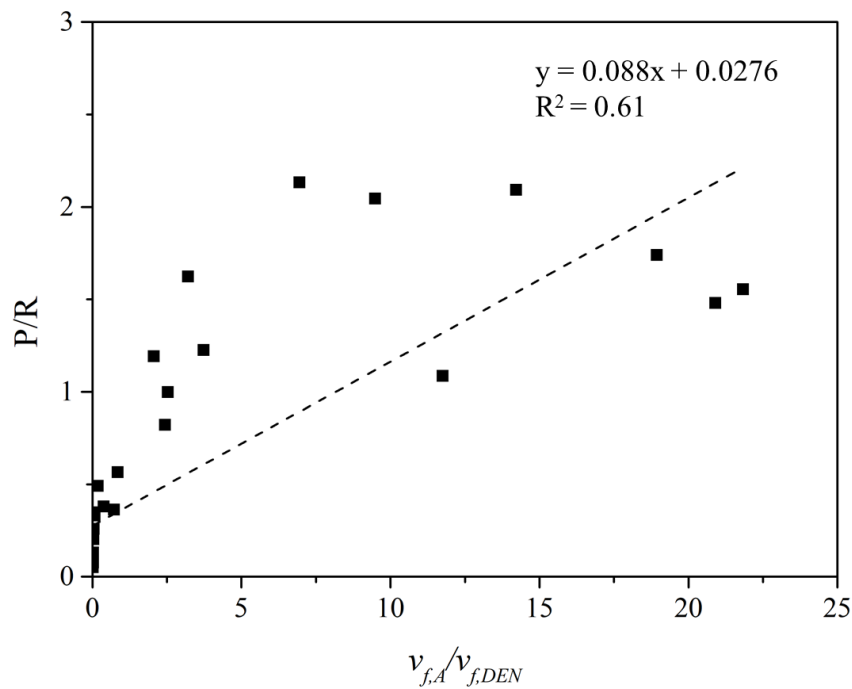


**Figure 4** Relationship between P/R and  $v_{f,A} / v_{f,DEN}$  ( $P/R = 0.088 \times v_{f,A} / v_{f,DEN} + 0.276$ ,  $R^2 = 0.61$ ,  $p < 0.05$ )

However, since PS discharges could influence the metabolism in different ways, the DIN retention pathways were dissimilarly regulated in the impacted reach. Based on the two examples (i.e., Reaches B and C) in the Nanfei River, the effects of two types of PS on the river metabolism and

the subsequent instream DIN retention pathways were distinctive. The discharge of untreated wastewater stimulated autotrophy and thereby enhanced assimilatory uptake, making it the main process of DIN retention. The discharge of WWTP effluent created a net heterotrophic ecosystem downstream, making Reach C a denitrification hotspot. Therefore, the impacts of PS inputs on DIN retention pathways cannot be generalized; rather, they are dictated by the impacts of PS inputs on river metabolism, which again depends on the PS discharge quantity and composition (i.e., wastewater treatment capacity and level).

#### *4.4. Effects of PS inputs on total DIN retention ratio*

Due to low DIN levels in the reference Reach A, DIN was most efficiently utilized by the uptake by biota. With the discharge of the untreated wastewater, though both the autotrophic and heterotrophic processes were enhanced in Reach B, the total DIN retention capacity was still impaired. Furthermore, Reach C, despite serving as a denitrification hotspot, had an even lower total DIN retention ratio than did Reach B, which indicated that the saturated DIN retention capacity via denitrification might be lower than that via assimilatory uptake in the Nanfei system. Our results demonstrated that the two types of PS inputs both impaired the total DIN retention capacities in receiving waters although they have very different discharge quantity and constituent compositions. The tertiary WWTP discharge still played the role of point source instead of 'point sink' to the N levels in the receiving water. Our finding supported the classic viewpoint that high DIN loading from PS inputs may cause instream DIN retention saturation (Bernot and Dodds, 2005; Haggard et al., 2005). In these cases, the proportion of DIN that was removed from transport declined, and more DIN was exported to the downstream ecosystem, potentially increasing its risk of algal bloom.

The Nanfei River enters Chaohu Lake, which serves as the only drinking water source for downstream Chaohu City. Algal blooms occur almost every year in Chaohu Lake (Hefei Bureau of Statistics, 2018), and they threaten the safety of the drinking water supply of Chaohu City. The declined total DIN retention capacity downstream from the WWTP means more N being transported to downstream ecosystems. Considering the negative impacts of DIN on the health of the ecosystem and the drinking water supply, engineered measures that reduce DIN inputs from PSs or increase instream DIN retention capacity are recommended for the Nanfei River.

## 5. Conclusions

In the present study, the 11-km urban reach of the Nanfei River was evaluated through the spatially intensive monitoring and Bayesian modeling approach under low-flow conditions. Based on the model results, the DIN retention ratios and pathways in the reference Reach A, wastewater-impacted Reach B, and effluent-dominated Reach C, were quantified and assessed. The discharge of untreated wastewater significantly increased the ambient  $\text{NH}_4^+$  concentration and promoted assimilatory  $\text{NH}_4^+$  uptake rate in Reach B. However, the assimilatory uptake efficiency decreased compared with the results observed in Reach A. The WWTP effluent significantly elevated the downstream  $\text{NO}_3^-$  concentrations in Reach C. The hypoxic conditions of the overlying water made denitrification possible in the water column, and the  $\text{NO}_3^-$  discharged in the effluent was delivered from the oxic to the hypoxic environment via longitudinal advection, which provided favorable conditions that made Reach C a denitrification hotspot. The ratio of total DIN retention via assimilatory uptake was 92% in Reach B, while the DIN retention becomes dominated by denitrification (91%) in Reach C. This indicated that the effects of point-source inputs on the DIN retention pathways cannot be simply generalized. They were

regulated by their effects on river metabolism. Despite the different DIN retention pathways, the total DIN retention ratios in Reach B ( $14.3\% \text{ km}^{-1}$ ) and C ( $6.5\% \text{ km}^{-1}$ ) were much lower than that in Reach A ( $30.3\% \text{ km}^{-1}$ ). Our findings corroborated that the instream DIN retention capacity reached saturation and was significantly impaired as a result of the effects of point-source inputs. It is implied that the DIN discharged from point-source inputs to urban rivers will influence the aquatic ecosystem not only locally but also more distant downstream. Therefore, the upgrading of WWTPs is undoubtedly the most direct way to alleviate N pollution in the systems where effluents contribute considerable N loadings. Our findings might also be helpful to the N management in water bodies in other regions with increasing mega-urbanization trend.

## **Acknowledgement**

This work was supported by China's Major Science and Technology Program for Water Pollution Control and Treatment (Grant No. 2013ZX07304-002). The authors would like to sincerely thank the Drainage Administration Office of Hefei City for their help with the sample collection and data collection in the Nanfei River. Dr. Jingshui Huang would like to appreciate CSC-DAAD Postdoc Fellowship for financially supporting her stay in UFZ, Germany.

## **Appendix A Supporting Information**

Supporting information contains the hydrograph in 2015, schematic description of N cycling in the model, hydrodynamic and water quality model validation results, parameter sensitivity ranking, longitudinal variations of more hydrodynamic and water quality variables, river metabolism and DIN flux balance.

## References

- Alexander, R.B., Böhlke, J.K., Boyer, E.W., David, M.B., Harvey, J.W., Mulholland, P.J., Seitzinger, S.P., Tobias, C.R., Tonitto, C. and Wollheim, W.M., 2009. Dynamic modeling of nitrogen losses in river networks unravels the coupled effects of hydrological and biogeochemical processes. *Biogeochemistry* 93, 91-116.
- Bernot, M.J. and Dodds, W.K., 2005. Nitrogen Retention, Removal, and Saturation in Lotic Ecosystems. *Ecosystems* 8, 442-453.
- Bowie, G.L., Mills, W.B., Porcella, D.B., Campbell, C.L., Pagenkopf, J.R., Rupp, G.L., Johnson, K.M., Chan, P.W.H. and Gherini, S.A., 1985. Rates, Constants, and Kinetics Formulations in Surface Water Quality Modeling (Second Edition), US EPA, Athens GA 30613 US.
- Carey, R.O. and Migliaccio, K.W., 2009. Contribution of Wastewater Treatment Plant Effluents to Nutrient Dynamics in Aquatic Systems: A Review. *Environmental Management* 44, 205-217.
- David, A., Perrin, J.-L., Rosain, D., Rodier, C., Picot, B. and Tournoud, M.-G., 2011. Implication of two in-stream processes in the fate of nutrients discharged by sewage system into a temporary river. *Environmental Monitoring and Assessment* 181, 491-507.
- Figuerola-Nieves, D., McDowell, W.H., Potter, J.D. and Martínez, G., 2015. Limited uptake of nutrient input from sewage effluent in a tropical landscape. *Freshwater Science* 35, 12-24.
- Gibson, C.A. and Meyer, J.L., 2007. Nutrient Uptake in a Large Urban River. *JAWRA Journal of the American Water Resources Association* 43, 576-587.
- Gücker, B., Brauns, M. and Pusch, M.T., 2006. Effects of wastewater treatment plant discharge on ecosystem structure and function of lowland streams. *Journal of the North American Benthological Society* 25, 313-329.
- Haggard, B.E., Stanley, E.H. and Storm, D.E., 2005. Nutrient retention in a point-source-enriched stream. *Journal of the North American Benthological Society* 24, 29-47.
- Huang, J., Xie, R., Yin, H. and Zhou, Q., 2018. Assessment of water quality and source apportionment in a typical urban river in China using multivariate statistical methods. *Water Science and Technology: Water Supply* 18, 1841-1851.
- Huang, J., Yin, H., Chapra, S.C., Zhou, Q., 2017. Modelling dissolved oxygen depression in an urban river in China. *Water* 9, 520-538.
- Huang, J., Yin, H., Jomma, S., Rode, M., Zhou, Q., 2016. Identification of pollutant sources in a rapidly developing urban river catchment in China. *EGU General Assembly* 2016.

554 Janse, J.H., Scheffer, M., Lijklema, L., Van Liere, L., Sloot, J.S., Mooij, W.M., 2010. Estimating the critical  
 555 phosphorus loading of shallow lakes with the ecosystem model PCLake: Sensitivity, calibration and  
 556 uncertainty. *Ecological Modelling* 221, 654-665.

557 Li, T., Qian, J., Shen, J., Ruan, D., 2014. Water quality monitoring and analysis of the overflow from the  
 558 drainage system in Hefei. *Water & Wastewater Engineering* 40, 40-44. (in Chinese)

559 Martí, E., Riera, J.L. and Sabater, F., 2010. Effects of Wastewater Treatment Plants on Stream Nutrient  
 560 Dynamics Under Water Scarcity Conditions. Sabater, S. and Barceló, D. (eds), pp. 173-195, Springer Berlin  
 561 Heidelberg, Berlin, Heidelberg.

562 Matott, L.S., 2005. OSTRICH – An Optimization Software Toolkit for Research Involving Computational  
 563 Heuristics Documentation and User's Guide Version 17.12.19. Department of Civil, Structural, and  
 564 Environmental Engineering, State University of New York at Buffalo, Buffalo, NY Available from  
 565 <http://www.eng.buffalo.edu/~lsmatott/Ostrich/OstrichMain.html>.

566 Ministry of Housing and Urban Rural Development China., 2014. Code for design of outdoor wastewater  
 567 engineering, China Plan Press, Beijing. (in Chinese)

568 Mulholland, P.J., Helton, A.M., Poole, G.C., Hall, R.O., Hamilton, S.K., Peterson, B.J., Tank, J.L., Ashkenas,  
 569 L.R., Cooper, L.W., Dahm, C.N., Dodds, W.K., Findlay, S.E.G., Gregory, S.V., Grimm, N.B., Johnson, S.L.,  
 570 McDowell, W.H., Meyer, J.L., Valett, H.M., Webster, J.R., Arango, C.P., Beaulieu, J.J., Bernot, M.J., Burgin,  
 571 A.J., Crenshaw, C.L., Johnson, L.T., Niederlehner, B.R., O'Brien, J.M., Potter, J.D., Sheibley, R.W., Sobota,  
 572 D.J., Thomas, S.M., 2008. Stream denitrification across biomes and its response to anthropogenic nitrate  
 573 loading. *Nature* 452, 202-U246.

574 NRE Incorporation., 2014. A Dynamic One-Dimensional Model of Hydrodynamics and Water Quality EPD-  
 575 RIV1 Version 2.1 Technical Manual, Georgia Environmental Protection Division, Atlanta, Georgia.

576 Peterson, B.J., Wollheim, W.M., Mulholland, P.J., Webster, J.R., Meyer, J.L., Tank, J.L., Martí, E., xe, nia,  
 577 Bowden, W.B., Valett, H.M., Hershey, A.E., McDowell, W.H., Dodds, W.K., Hamilton, S.K., Gregory, S.,  
 578 Morrall, D.D., 2001. Control of Nitrogen Export from Watersheds by Headwater Streams. *Science* 292, 86-  
 579 90.

580 Pianosi, F., Sarrazin, F., Wagener, T., 2015. A Matlab toolbox for Global Sensitivity Analysis. *Environmental*  
 581 *Modelling & Software* 70(Supplement C), 80-85.

582 Rahm, B.G., Hill, N.B., Shaw, S.B., Riha, S.J., 2016. Nitrate Dynamics in Two Streams Impacted by  
 583 Wastewater Treatment Plant Discharge: Point Sources or Sinks? *JAWRA Journal of the American Water*  
 584 *Resources Association* 52, 592-604.

585 Raimonet, M., Vilmin, L., Flipo, N., Rocher, V., Laverman, A.M., 2015. Modelling the fate of nitrite in an  
 586 urbanized river using experimentally obtained nitrifier growth parameters. *Water Research* 73, 373-387.  
 587 Seitzinger, S., Harrison, J.A., xf, hlke, J.K., Bouwman, A.F., Lowrance, R., Peterson, B., Tobias, C., Van Drecht,  
 588 G., 2006. Denitrification across Landscapes and Waterscapes: A Synthesis. *Ecological Applications* 16,  
 589 2064-2090.  
 590 Hefei Bureau of Statistics, Hefei Statistics Survey Team of National Bueau, 2018. 2018 Hefei Statistical  
 591 Yearbook, China Statistics Press, Beijing. (in Chinese)  
 592 Tank, J.L., Reisinger, A.J., Rosi, E.J., 2017. Nutrient limitation and uptake. *Methods in Stream Ecology:*  
 593 *Volume 2: Ecosystem Function*, 147.  
 594 Vrugt, J.A., 2016. Markov chain Monte Carlo simulation using the DREAM software package: Theory,  
 595 concepts, and MATLAB implementation. *Environmental Modelling & Software* 75, 273-316.  
 596 Wagenschein, D., Rode, M., 2008. Modelling the impact of river morphology on nitrogen retention—A  
 597 case study of the Weisse Elster River (Germany). *Ecological Modelling* 211, 224-232.  
 598 Wool, T.A., Ambrose, R.B., Martin, J.L., Comer, E.A., 2002. Water Quality Analysis Simulation Program  
 599 (WASP) Version 6.0 DRAFT: User's Manual, US Environmental Protection Agency – Region 4, Atlanta, GA,  
 600 US.  
 601 Yu, C., Huang, X., Chen, H., Godfray, H.C.J., Wright, J.S., Hall, J.W., Gong, P., Ni, S., Qiao, S., Huang, G., Xiao,  
 602 Y., Zhang, J., Feng, Z., Ju, X., Ciais, P., Stenseth, N.C., Hessen, D.O., Sun, Z., Yu, L., Cai, W., Fu, H., Huang, X.,  
 603 Zhang, C., Liu, H., Taylor, J., 2019. Managing nitrogen to restore water quality in China. *Nature*.

1

## APPENDIX A

2

### SUPPORTING INFORMATION

3

for

4

**Modeling the impacts of point-source inputs on nitrogen**

5

**retention in an urban river under low-flow conditions**

6

Jingshui Huang <sup>1,2</sup>, Hailong Yin <sup>1,\*</sup>, Seifeddine Jomaa <sup>2</sup>, Michael Rode <sup>2</sup>, Qi Zhou <sup>1</sup>

7

<sup>1</sup> College of Environmental Science and Engineering, Tongji University, Shanghai 200092, China.

8

<sup>2</sup> Department of Aquatic Ecosystem Analysis and Management, Helmholtz Centre for

9

Environmental Research – UFZ, Brückstraße 3a, 39114 Magdeburg, Germany.

10

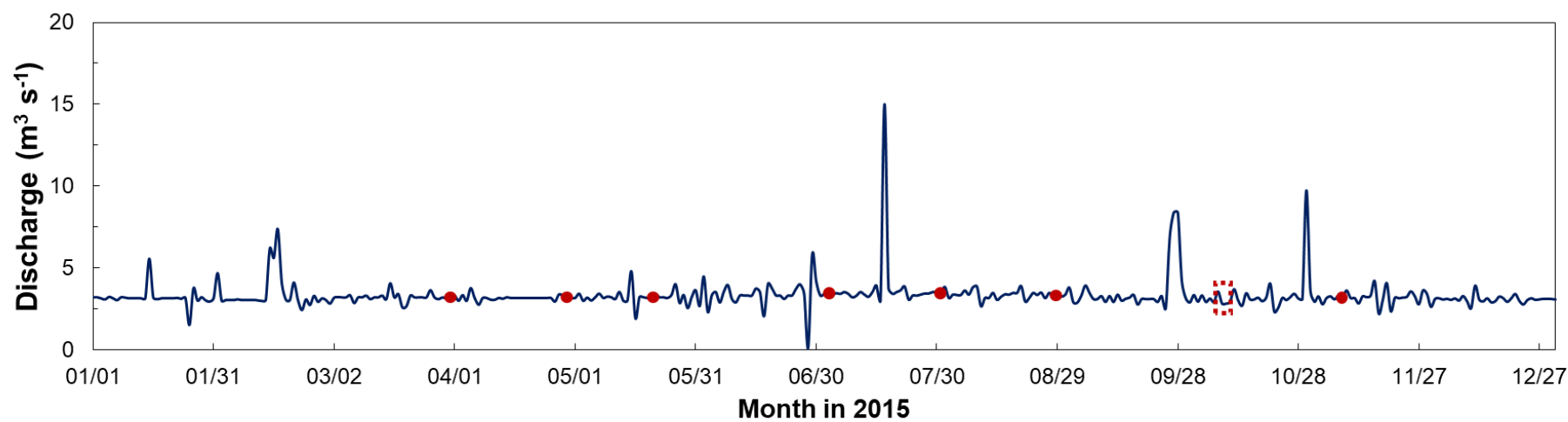
11

\* Author to whom all correspondence should be addressed: [yinhailong@tongji.edu.cn](mailto:yinhailong@tongji.edu.cn);

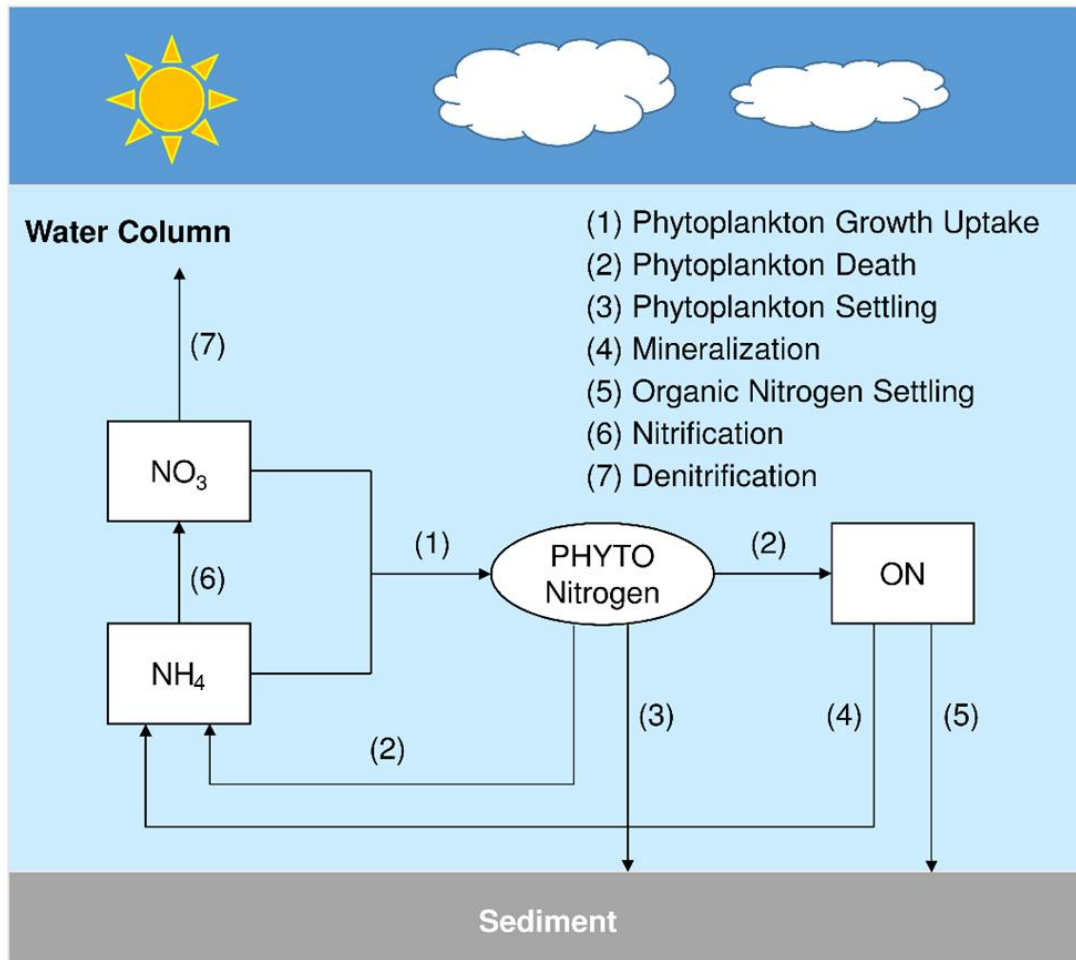
12

13

Supporting Information consists of 8 figures and 1 table.



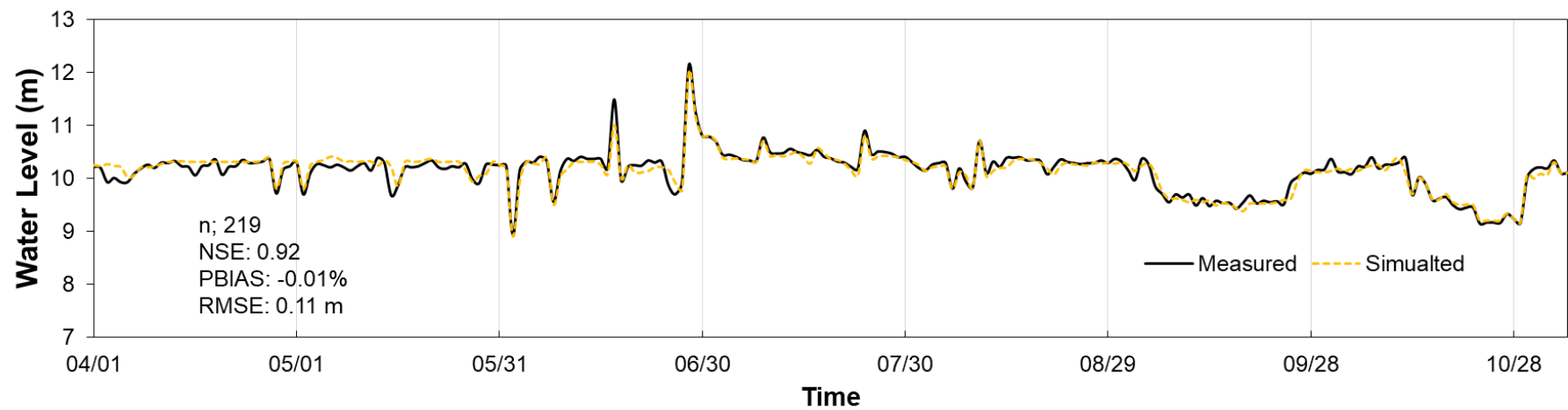
14  
 15 **Figure S1** Discharge hydrograph at Site 14 in the Nanfei River for the year 2015. The red dots represent the routine sampling dates. The red  
 16 dashed square represents the intensive Lagrange survey under low-flow condition.



17

18

**Figure S2** Schematic description of the N cycling in the WASP EUTRO Module.



19

20 **Figure S3** Results of hydrodynamic model validation: comparison of simulated and measured values of water level at Site 14 during 1<sup>st</sup> April - 5<sup>th</sup>  
 21 November 2015; the number of measurements was 219.

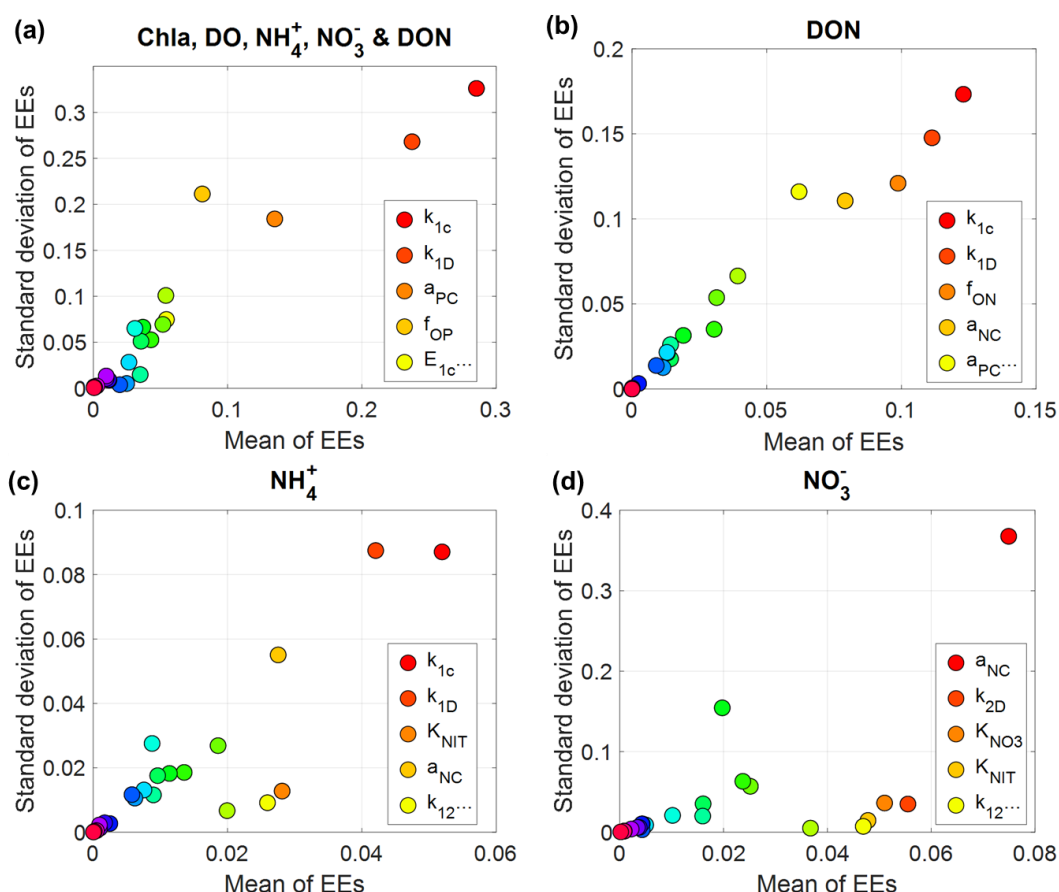


**Figure S4** Parameter sensitivity ranking by Elementary Effects (EE) method with different objective functions defined respectively by (a) the sum of NSE coefficients of  $\text{NH}_3$ ,  $\text{NO}_3$ , DON, Chl-a and DO, the NSE of (b) DON, (c)  $\text{NH}_3$ , and (d)  $\text{NO}_3$ . The more to the right a point along the horizontal axis, the more influential the parameters. The higher up a point along the vertical axis, the larger its degree of interactions with other parameters. Useful for screening and ranking. (Pianosi et al. 2016) The 5 most sensitive parameters for each objective function are shown in its legend.

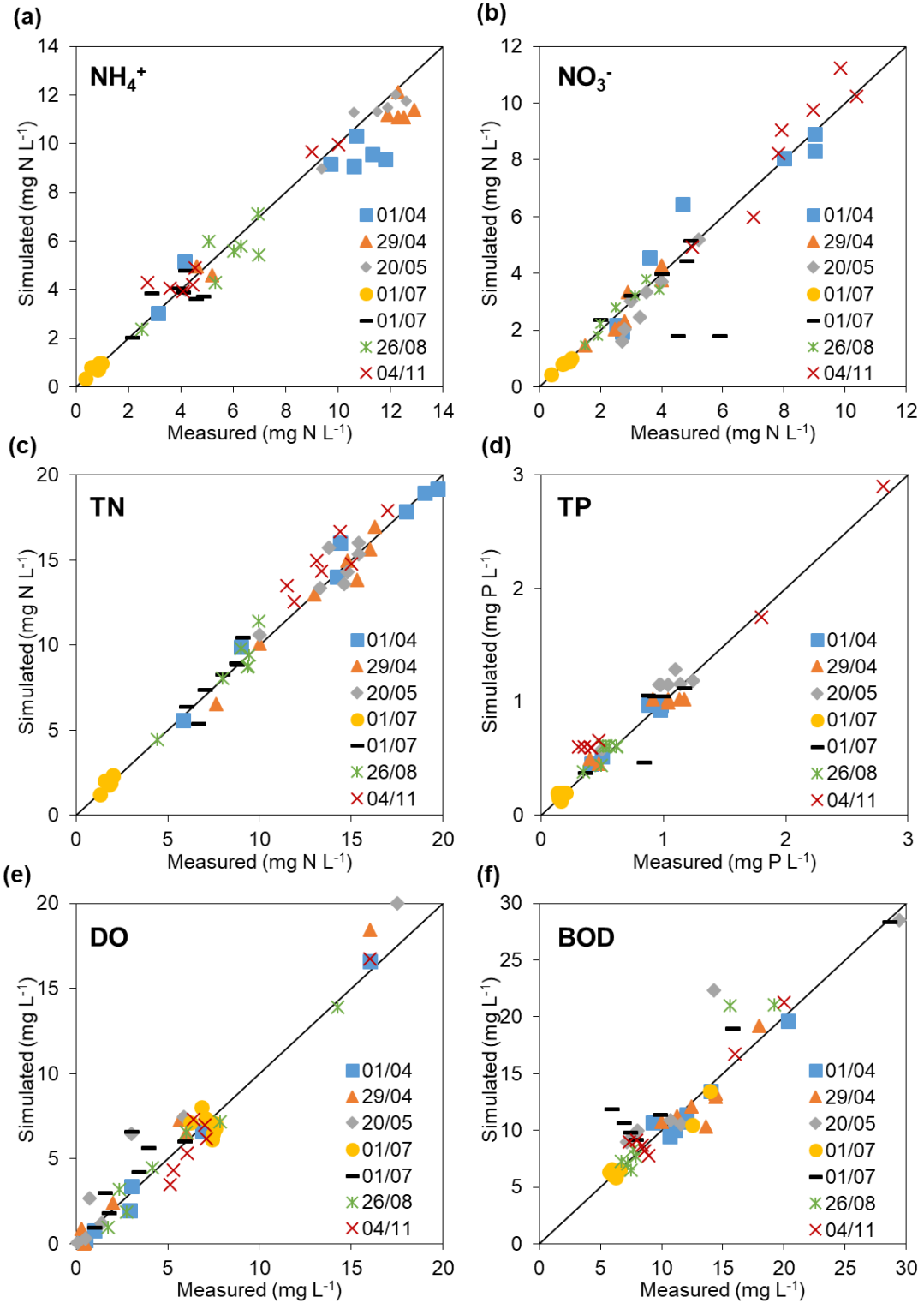


**Figure S5** Results of hydrodynamic model validation: comparison of simulated and measured values of water level at Site 14 during 1<sup>st</sup> April - 5<sup>th</sup> November 2015; the number of measurements was 219.

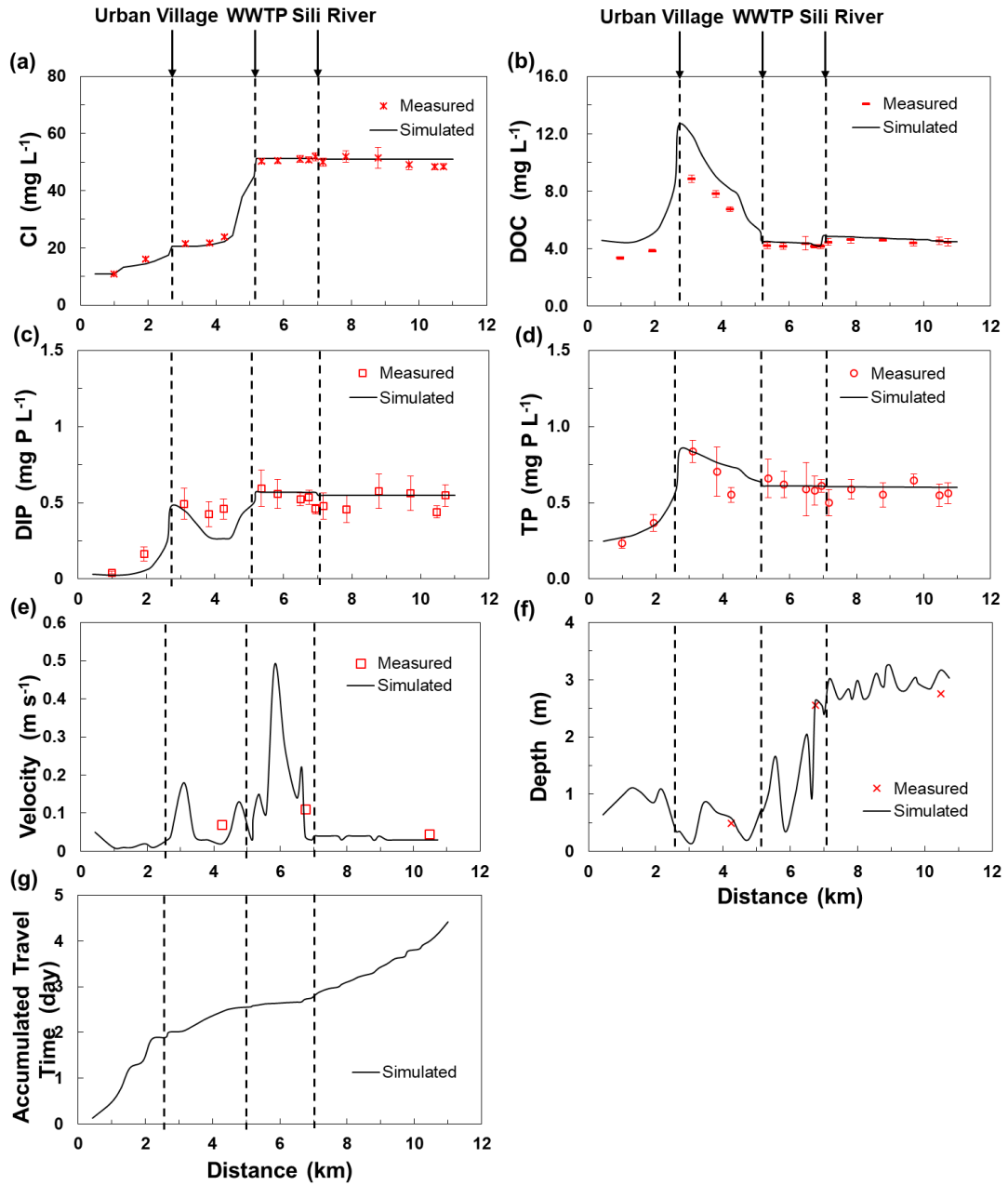
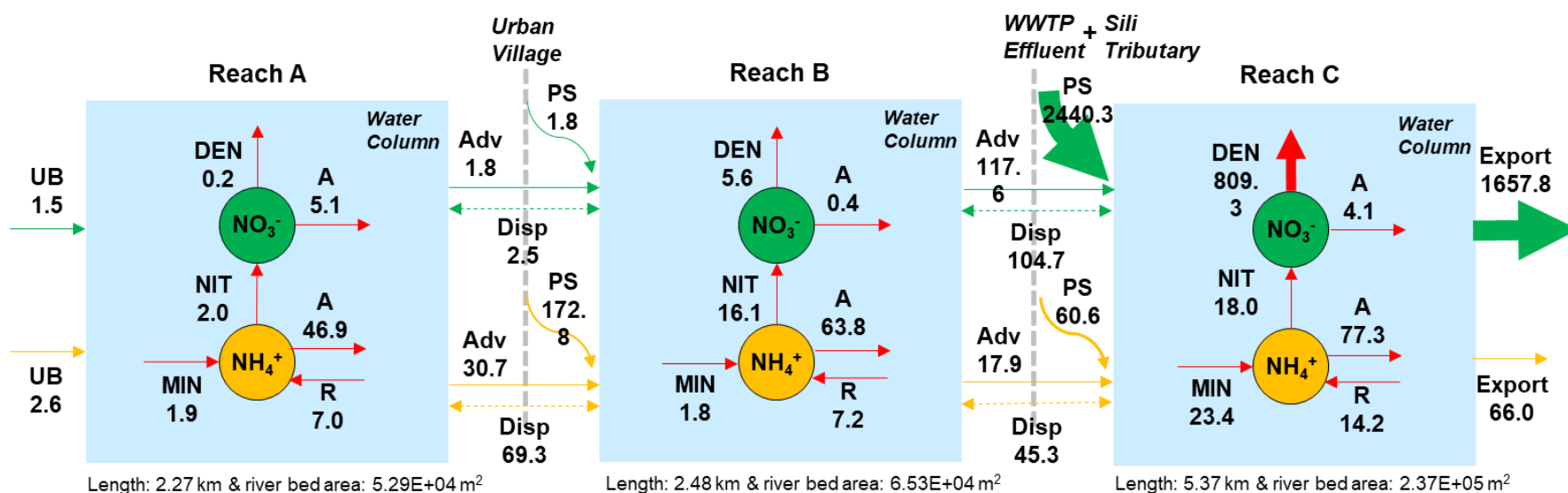


**Figure S6** Longitudinal measured and simulated (a) Cl (b) DOC (c) DIP (d) TP (e) velocity (f) depth and simulated (f) accumulated travel time during low-flow conditions in the Nanfei River.

38

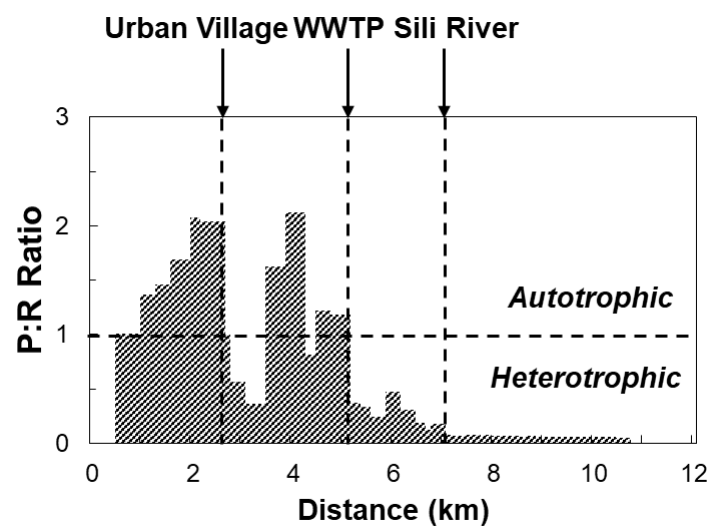


39

**Figure S7** DIN mass balance fluxes (kg N d<sup>-1</sup>) including boundaries, advections, dispersions, loadings, reactions and exports in Reaches A, B and C;

40

UB, Adv and Disp are short for upper boundary, advective and dispersive transport, respectively.



41  
 42 **Figure S8** Longitudinal primary production to respiration ratio and metabolism  
 43 condition (Huang et al. 2017)

44 **Table S1.** DIN cycling, inputs & exports fluxes (kg N d<sup>-1</sup>) in the three representative  
 45 reaches and whole reach.

Flux	Reach A		Reach B		Reach C		Whole Reach	
	NH <sub>4</sub> <sup>+</sup>	NO <sub>3</sub> <sup>-</sup>	NH <sub>4</sub> <sup>+</sup>	NO <sub>3</sub> <sup>-</sup>	NH <sub>4</sub> <sup>+</sup>	NO <sub>3</sub> <sup>-</sup>	NH <sub>4</sub> <sup>+</sup>	NO <sub>3</sub> <sup>-</sup>
Inputs								
Upper Boundary	1.5	2.6	30.7	1.8	17.9	117.6	1.5	2.6
Urban village			172.8	3.5			172.8	3.5
WWTP					19.5	1757.4	19.5	1757.4
Sili River					41.0	682.9	41.0	682.9
Dispersion	69.3	2.5	-114.6	102.2	45.3	-104.7		
Σ Inputs	70.8	5.1	88.9	107.4	123.7	2453.2	234.8	2446.3
Processes								
Mineralization	1.9		1.8		23.4		27.0	
Nitrification	-2.0	2.0	-16.1	16.1	-18.0	18.0	-36.1	36.1
Phytoplankton death	7.0		7.2		14.2		28.4	
Assimilatory uptake	-46.9	-5.1	-63.8	-0.4	-77.3	-4.1	-188.0	-9.6
Denitrification		-0.2		-5.6		-809.3		-815.1
Σ Processes	-40.1	-3.3	-71.0	10.2	-57.7	-795.4	-168.7	-788.6
Export	30.7	1.8	17.9	117.6	66.0	1657.8	66.0	1657.8

46

47   **References**

- 48   Huang, J., Yin, H., Chapra, S.C. and Zhou, Q. (2017) Modelling dissolved oxygen  
49   depression in an urban river in China. *Water* (9).
- 50   Pianosi, F., Beven, K., Freer, J., Hall, J.W., Rougier, J., Stephenson, D.B. and Wagener, T.  
51   (2016) Sensitivity analysis of environmental models: A systematic review with practical  
52   workflow. *Environmental Modelling & Software* 79(Supplement C), 214-232.  
53